A Numerical and Experimental Simulation Study of the Fluid Flow Characteristics of the Past Horizontal Stabilizer and Elevator of the Microlight Aircraft Model

Nasaruddin Salam
Mechanical Engineering Department, Faculty of Engineering, Hasanuddin University, Indonesia
nassalam.unhas@yahoo.co.id

Rustan Tarakka
Mechanical Engineering Department, Faculty of Engineering, Hasanuddin University, Indonesia
rustan_tarakka@yahoo.com

Lukman Kasim
Mechanical Engineering Department, Faculty of Engineering, Hasanuddin University, Indonesia
lukman.kasim@unhas.ac.id (corresponding author)

Received: 20 December 2024 | Revised: 2 February 2025 | Accepted: 6 February 2025

 DOI: https://doi.org/10.48084/etasr.9982

ABSTRACT

A microlight aircraft named PPH-Unhas was developed at Hasanuddin University in Makassar, Indonesia, in 2020. This study aims to produce the characteristics of the lift coefficient (C_L), drag coefficient (C_D), and flow simulation on the horizontal stabilizer and elevator model of the PPH-Unhas microlight aircraft. Numerical simulations were conducted using a Computational Fluid Dynamics (CFD) program, and experiments were performed in a low-speed wind tunnel. The microlight aircraft model was made of three pieces adapted to the PPH-Unhas aircraft prototype and then tested by treating five levels of airflow velocity (V): 14, 16, 18, 20, and 22 m/s. Each speed level was treated with seven levels of angle of attack (α), namely, -15°, -5°, 0°, 10°, 15°, 20°, and 25°. Each α level was treated with six levels of change in the aircraft elevator deflection angle (δ): -15°, 0°, 10°, 20°, 30°, and 45°. The results showed that the maximum values of C_D and C_L were obtained at δ = 45°, whereas the maximum value of C_L/C_D was obtained at δ = 45°.

Keywords-stabilizer and elevator model; lift coefficient; drag coefficient; flow contours

I. INTRODUCTION

Hasanuddin University Makassar Indonesia 2020 developed a microlight aircraft to assist in the development of ultralight aircrafts. This aircraft was named PPH-Unhas. The prototype microlight aircraft can carry two passengers and 75 kg of luggage. The aircraft wing model was tested in the Fluid Mechanics Laboratory. Previous experimental investigations have revealed that curved plates exhibit superior aerodynamic performance compared to thin plates [1]. The lift, drag, and pitching moment at the quarter chord for various curved and thin plate configurations were evaluated within a Reynolds number range of 60,000 to 200,000. In addition, no evidence of hysteresis, which is commonly observed in thick wings or airfoils, has been detected [1].

Research on the swayasa aircraft wing, based on the NACA 23012 airfoil and the PPH-Unhas prototype, deployed CFD and subsonic wind tunnel experiments. The results exhibited that increasing the flap angle increased the maximum C_L and C_D, with a C_L/C_D ratio of 1.5501 at flap angles of 0° and 15° [2].

Studies using numerical and experimental methods have examined the behavior of horizontal stabilizer systems under extreme aerodynamic loading conditions. A good agreement was reached between the findings of the computational and experimental tests conducted to evaluate the mechanical strength of these stabilizers [3]. Research on horizontal stabilizers and aircraft elevators has demonstrated that a higher elevator deflection angle increases the C_L. For α = 2° and an elevator deflection angle of 20°, C_L = 0.93 (gap length 1.75%). In addition, C_L = 1.83 (gap length of 2%) for the horizontal stabilizer at an angle of 10° [4].

The lift coefficient impacts are caused by elevator deflection, demonstrating how changes in different parameters

influence the aircraft's reaction to the latter. The control surface deflection causes the lift and moment to rise or decrease. The ANSYS 12.0 FLUENT software was implemented for the analysis, and CATIA V5 was utilized to develop several equations for longitudinal stability and control, as well as for the design of horizontal stabilizers and elevators [5].

CFD can predict the aerodynamic advantages of smooth wings over traditional designs. The impact of a flexible wing on the horizontal stabilizer was explored in [6]. Eliminating the rivets and cleats that secure the elevator to the stabilizer significantly reduces the drag. Additionally, a stabilizer designed without conventional control surfaces, relying instead on trailing-edge deflection for movement, enhances the maneuverability [6].

A linearized aircraft model simplifies the controller design for servomotor dynamics in longitudinal control and gyro modeling for the roll control of an F-16. The MATLAB Simulink© analysis shows that the Fuzzy-PID controller performs best for longitudinal and roll motions [7]. The proposed design increases the trimmable horizontal stabilizer load, boosting flight efficiency by enabling a 21% increase in the payload, an extended range, reduced thrust, or smaller wings. These benefits provide operational and economic advantages [8].

A study on the aerodynamic performance of a bioinspired morphing Micro Air Vehicle (MAV) with an adaptive wing structure used CFD simulations in Ansys Fluent 15.0 and experimental tests with particle image velocimetry in a low-speed wind tunnel. The MAV, a Zimmerman wing with an Eppler 61 airfoil, was tested across three wing configurations with varying curvatures and thicknesses at all angles of attack. The lift coefficient, C_L, drag coefficient C_D, and aerodynamic efficiency C_L/C_D analyses were utilized to identify the optimal configuration for performance [9].

Additionally, experiments with a Cross-Flow Fan (CFF) demonstrated exceptional airflow control, achieving lift coefficients of over 7.6 and propulsion coefficients of over 7.1 at high angles of attack (30°–40°) and low airspeeds. The CFF delays flow separation, creates vortex-induced lift and thrust through eccentric vortices, and improves performance depending on the advance ratio and angle of attack, with lift and thrust increasing as these parameters increase [10].

An algorithm for elevator sizing in aircraft design software provides formulas for achieving longitudinal control and trimming, with a solved example for clarity [11]. The seamless wing concept improves horizontal stabilizers by removing rivets and cleats, reducing drag, and enhancing maneuverability through trailing-edge deflection, instead of traditional control surfaces [12]. Additionally, the use of observers significantly reduces the pitch angle deviation (0.08 radians with observers vs. 0.2 radians without observers), improving stability and minimizing the risk of destabilizing motion along the x-axis [13].

A CFD study analyzed water droplet wakes and aerodynamic characteristics of the PzL-106 "Kruk" agricultural aircraft using RANS simulations with k-ω SST and Spalart-Allmaras turbulence models. The results highlighted the flow separation regions and were validated against experimental data, offering insights beyond the wind tunnel limitations [14].

Another study examined the effects of tip vorticity on laminar separation bubbles over an NACA 4412 airfoil at Re = 50,000. The visualization exhibited reduced bubbles on low-aspect-ratio wings as the angle of attack increased, whereas higher aspect ratios lowered the stall angles [15].

Research has also emphasized the importance of modeling control surface tabs early in the design process to address critical flutter and mitigate risks through timely adjustments [16].

Aircraft balancing during short, straight-line landings was explored using separate rudders and elevators as air brakes. Two methods were proposed: manual or automatic trimming of the pitching, yawing, and rolling moments, and redesigning the elevator control channels to limit the deflection angles [17].

Another study developed a longitudinal aerodynamic model for general aviation aircraft at high angles of attack using the strip theory and non-linear lift line theory to calculate aerodynamic forces and moments, including elevator deformation effects. Validation was performed utilizing wind tunnel data for a single-engine, low-wing aircraft [18].

Research on ground effect phenomena introduced a methodology for estimating the downwash angle, effective angle of attack, aerodynamic force variations, and elevator requirements for trimming. This method accurately predicts these trends [19].

At a certain speed, the pilot begins to move the elevator with a deflection of the aircraft rotation to increase the angle of attack, thereby increasing the lift coefficient. The maximum angle of attack achieved during rotation should not exceed the angle of attack at rest. All that is needed is that the angle of attack is high enough to produce a lift force at a certain speed greater than its weight, so that the plane will take off from the ground [20].

Previous research on the aerodynamic interaction between the horizontal stabilizer and elevator when the aircraft is at various angles of attack and speeds is lacking. Therefore, research on how horizontal stabilizers and elevator changes affect the dynamic stability of microlight aircraft has not been conducted. In addition, research results on how the shape and angle of the horizontal stabilizer and elevator affect the lift and drag coefficients can be used by designers to optimize flight performance under various conditions.

In connection with the above, PPH-Unhas microlight aircraft research continues to obtain findings that can encourage innovation in small aircraft technology and become a reference for design techniques that can improve flight efficiency and effectiveness.

II. METHODOLOGY

The research was conducted via numerical simulation with a CFD program using Autodesk Fusion 360, Gambit 2.4.6, and Fluent 6.3.26 software. The experiments were conducted in a low-speed wind tunnel. The microlight aircraft model was

adjusted to the PPH-Unhas aircraft prototype and tested by treating five levels of airflow velocities (V): 14, 16, 18, 20, and 22 m/s. Each speed level was treated with seven levels of attack (α): -15°, -5°, 0°, 10°, 15°, 20°, and 25°. Each α level was treated with six levels of change in the aircraft elevator deflection angle (δ): -30°, -15°, 0°, 15°, 30°, and 45°.

The horizontal stabilizer and elevator aircraft models (test specimens) were constructed at a scale of 1:40. The size was adjusted to the available wind tunnel test section to obtain good test data, and the ratio of the cross-sectional area of the test object to that of the channel or wind tunnel test section should not be greater than 1:3. For this reason, the size is as shown in Figure 1. The test specimen was made of polycarbonate with a thickness of 1.75 mm. The treatment of the speed level, angle of attack, and elevator angle was the same in the numerical and experimental simulation methods. The dimensions of the PPH-Unhas microlight aircraft prototype are depicted in Figure 1, and those of the horizontal stabilizer and elevator model are portrayed in Figure 2. Figure 3 displays the low-speed wind tunnel in which the experiments were conducted.

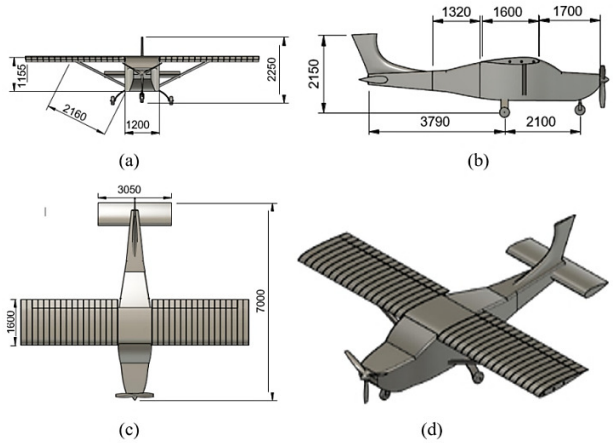

Fig. 1. The prototype size of the PPH-Unhas microlight aircraft, (a) front view, (b) side view, (c) top view, and (d) isometric view.

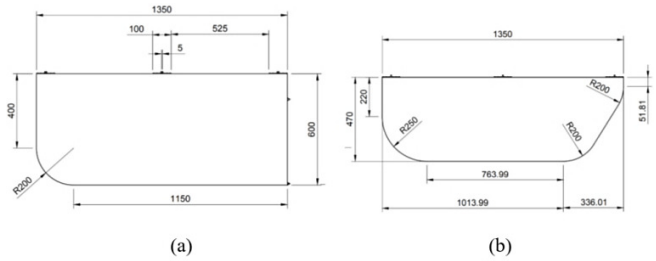

Fig. 2. Size of PPH-Unhas microlight aircraft model: (a) horizontal stabilizer and (b) elevator.

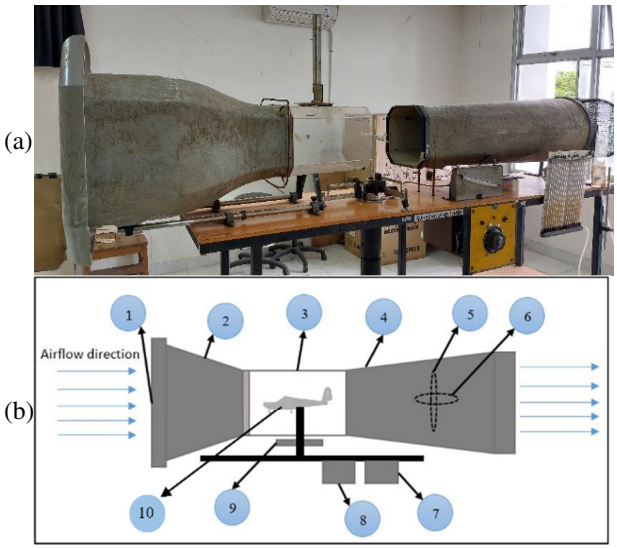

Fig. 3. Research equipment: (a) the subsonic wind tunnel equipment, and (b) test item model position. 1. Intake, 2. Diffuser, 3. Test section, 4. Diverging section, 5. Fan, 6. Electric motor, 7. Flow meter, 8. Voltage regulator, 9. Force balance measurements, 10. Test object.

The drag coefficient C_D can be determined using [21]:

$$C_D = \frac{F_D}{\frac{1}{2}\rho V^2 A} \quad (1)$$

where F_D is the drag force, ρ is the density, V is the air velocity, and A is the surface area of the test object. The lift coefficient C_L can be determined using [21]:

$$C_L = \frac{F_L}{\frac{1}{2}\rho V^2 A} \quad (2)$$

The magnitude of the Reynolds number is determined by [21]:

$$Re = \frac{\rho.V.D}{\mu} \quad (3)$$

Where D is the hydraulic diameter, and μ is the dynamic viscosity of the airflow.

III. RESULTS AND DISCUSSION

The experimental results of the drag force F_D were obtained by giving the same treatment of five levels of airflow velocity V of 14, 16, 18, 20, and 22 m/s, and six levels of elevator deflection angle (δ) from -30° to 45°. The experimental results are listed in Table I, and the analysis results are outlined in Table II, where the drag coefficient C_D was obtained.

Based on Tables I and II, Figures 4 and 5 show the relationship between F_D and C_D, with the elevator deflection angle δ for each speed level at an angle of attack α = 0°. The characteristic pattern is the same, and the largest F_D value of 0.550 N is obtained at δ = 45° and airflow velocity V = 22 m/s, whereas the largest C_D value is 0.681 at δ = 45° and airflow velocity V = 20 m/s.

TABLE I. DRAG FORCE (F_D) AT ANGLE OF ATTACK $A = 0^\circ$ WITH 5 LEVELS OF SPEED AND 6 LEVELS OF ELEVATOR DEFLECTION ANGLE (Δ)

V (m/s)	$F_{D\ Experiment}$ (N) at elevator deflection angle, δ (degree)					
	-30	-15	0	15	30	45
14	0.160	0.150	0.160	0.170	0.200	0.230
16	0.210	0.190	0.200	0.220	0.260	0.300
18	0.260	0.240	0.250	0.280	0.330	0.380
20	0.330	0.310	0.390	0.400	0.430	0.480
22	0.400	0.370	0.450	0.470	0.510	0.550

TABLE II. DRAG FORCE (F_D) AT ANGLE OF ATTACK $A = 0^\circ$ WITH 5 LEVELS OF SPEED AND 6 LEVELS OF ELEVATOR DEFLECTION ANGLE (Δ)

V (m/s)	$C_{D\ Experiment}$ on elevator deflection angle, δ (degree)						Re
	-30	-15	0	15	30	45	
14	0.480	0.467	0.521	0.529	0.599	0.666	151502
16	0.482	0.453	0.498	0.525	0.597	0.665	173146
18	0.471	0.452	0.492	0.528	0.598	0.665	194789
20	0.485	0.473	0.622	0.610	0.632	0.681	216432
22	0.485	0.467	0.593	0.593	0.619	0.645	238075

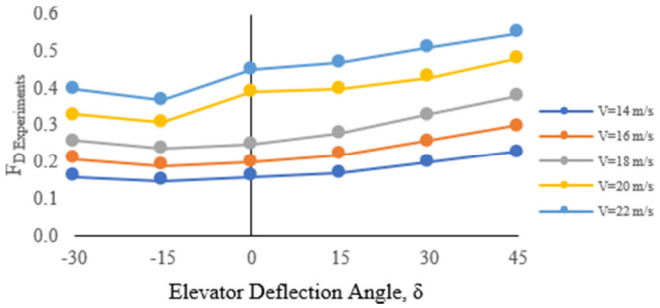

Fig. 4. Relationship between experimental drag force F_D and change in elevator deflection angle δ at angle of attack $\alpha = 0^\circ$ for each level of flow velocity change.

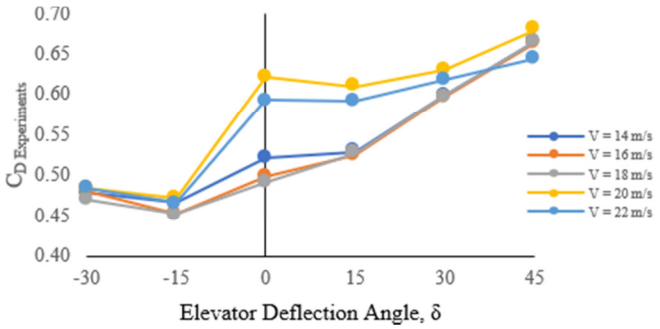

Fig. 5. Relationship of experimental C_D drag coefficient and change in elevator deflection angle δ at angle of attack α = 0° for each level of flow velocity change.

Figures 6 and 7 display the relationship between F_D and C_D, with the elevator deflection angle δ for each speed level at an angle of attack $\alpha = 10^\circ$. The characteristic pattern is the same, and the largest F_D value of 0.600 N is obtained at $\delta = 45^\circ$ and airflow velocity $V = 22$ m/s, whereas the largest C_D value is 0.7589 at $\delta = 45^\circ$ and airflow velocity $V = 18$ m/s. These results show an increase in the F_D and C_D values compared with the angle of attack $\alpha = 0^\circ$.

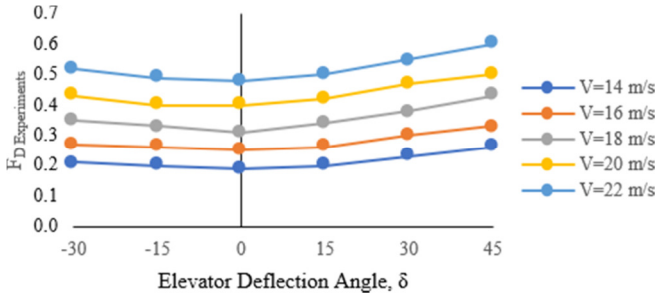

Fig. 6. Relationship between experimental drag force F_D and change in elevator deflection angle δ at angle of attack $\alpha = 10^\circ$ for each level of change in flow velocity.

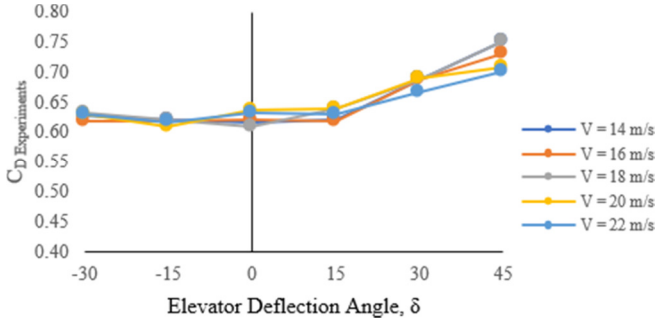

Fig. 7. Relationship of experimental C_D drag coefficient and change in elevator deflection angle δ at angle of attack $\alpha = 10^\circ$ for each level of flow velocity change.

Figures 8 and 9 demonstrate the relationship between F_D and C_D, with the elevator deflection angle δ for each speed level at an angle of attack $\alpha = 15^\circ$. The characteristic pattern is the same, and the largest F_D value of 1.040 N is obtained at $\delta = -30^\circ$ and airflow speed $V = 22$ m/s, whereas the largest C_D value is 1.297 at $\delta = -15^\circ$ and airflow speed $V = 20$ m/s. These results show an increase in the F_D and C_D values compared with the angle of attack $\alpha = 10^\circ$, and the elevator deflection angle, which produced the largest value, occurrs at a negative deflection angle.

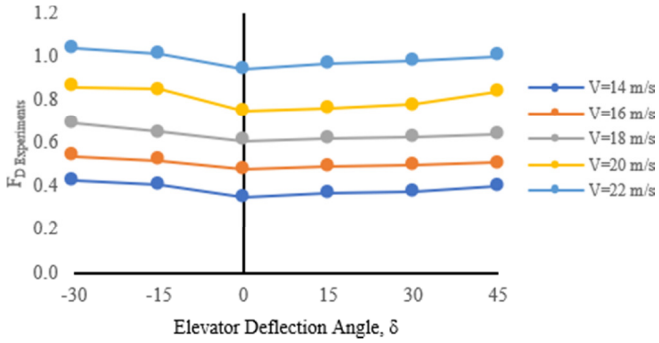

Fig. 8. Relationship of experimental drag force F_D and change in elevator deflection angle δ at angle of attack $\alpha = 15^\circ$ for each level of flow velocity change.

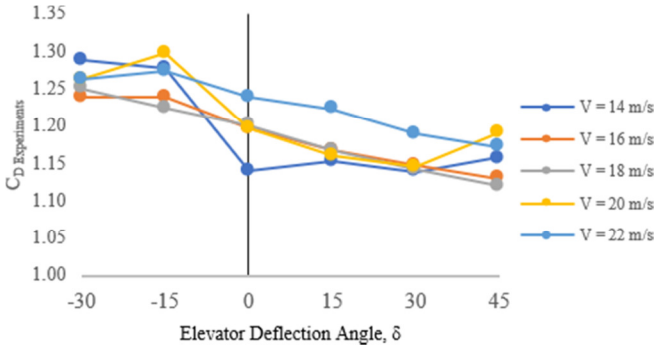

Fig. 9. Relationship between experimental C_D drag coefficient and change in elevator deflection angle δ at angle of attack α = 15° for each level of flow velocity change.

Figures 10 and 11 illustrate the relationship between F_D and C_D, with the elevator deflection angle δ for each speed level at an angle of attack α = 20°. The characteristic pattern is the same, and the largest F_D value of 1,300 N is obtained at δ = -30° and airflow velocity V = 22 m/s, while the largest C_D value is 1,578 at δ = -30° and airflow velocity V = 22 m/s. These results exhibit an increase in the F_D and C_D values compared to the angle of attack α = 15°, and the elevator deflection angle, which produces the largest value, also occurs at a negative deflection angle.

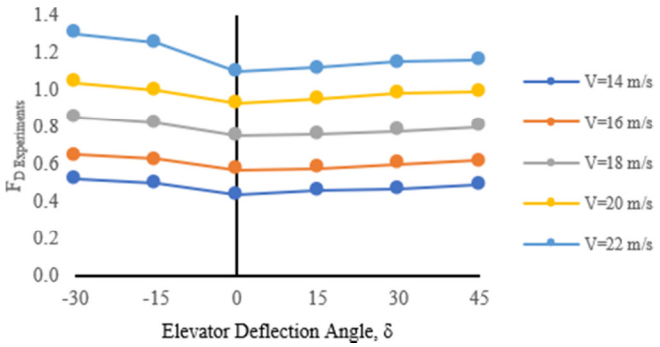

Fig. 10. Relationship between experimental drag force FD and change in elevator deflection angle δ at angle of attack α = 20 °for each level of flow velocity change.

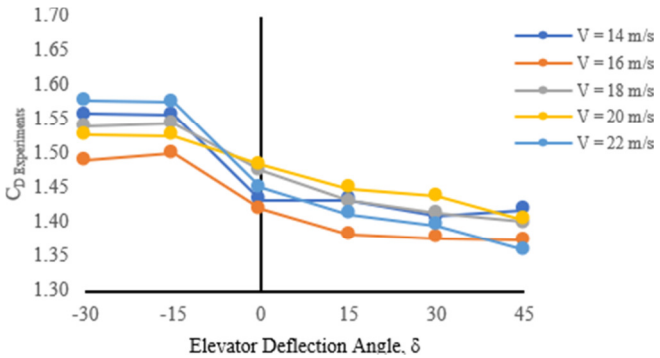

Fig. 11. Relationship between experimental C_D drag coefficient and change in elevator deflection angle δ at an angle of attack α = 20° for each level of flow velocity change.

Figures 12 and 13 portray the relationship between F_D and C_D, with the elevator deflection angle δ for each speed level at an angle of attack α = 25°. The characteristic pattern shown is the same, and the largest F_D value of 1,800 N is obtained at δ = -30° and airflow velocity V = 22 m/s, whereas the largest C_D value is 2,185 at δ = -30° and airflow velocity V = 22 m/s. These results exhibit an increase in the F_D and C_D values compared to the angle of attack α = 20°, and the elevator deflection angle, which produces the largest value, also occurs at a negative deflection angle.

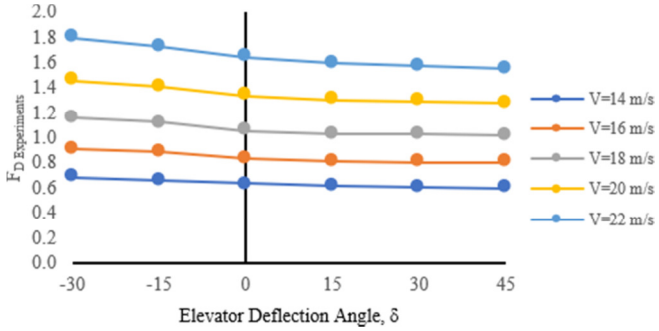

Fig. 12. Relationship between experimental drag force F_D and change in elevator deflection angle δ at angle of attack α = 25° for each level of flow velocity change.

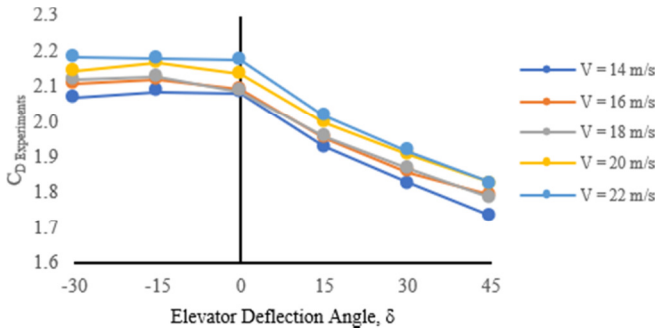

Fig. 13. Relationship between experimental C_D drag coefficient and change in elevator deflection angle δ at angle of attack α = 25° for each level of flow velocity change.

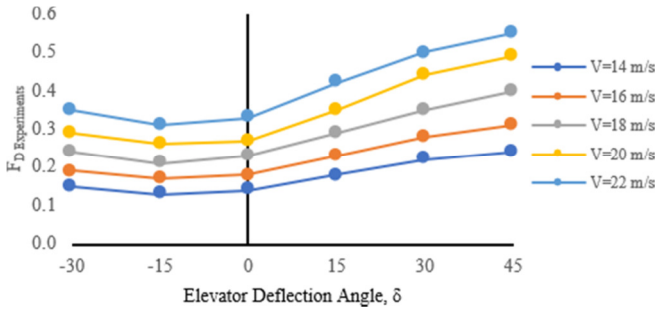

Fig. 14. Relationship of experimental drag force F_D and change in elevator deflection angle δ at angle of attack α = -5° for each level of flow velocity change.

Figures 14 and 15 display the relationship between F_D and C_D, with elevator deflection angle δ for each speed level at an angle of attack α = -5°. The characteristic pattern is similar, and the largest F_D value of 0.550 N is obtained at δ = 45° and

airflow velocity V = 22 m/s, whereas the largest C_D value is 0.695 at δ = 45° and airflow velocity V = 20 m/s. These results show an increase in the C_D value when compared to the angle of attack α = 0°. The elevator deflection angle, which produces the largest value, also occurs at a positive deflection angle. Figures 16 and 17 show the relationship between F_D and $C_{D,}$ with the elevator deflection angle δ for each speed level at an angle of attack α = -15°. The characteristic pattern is the same, and the largest F_D value of 0.590 N is obtained at δ = 45° and airflow velocity V = 22 m/s, whereas the largest C_D value is 0.752 at δ = 45° and airflow velocity V = 14 m/s. These results show an increase in *the* F_D and C_D values when compared to the angle of attack α = -5°, and the elevator deflection angle, which produces the largest value, also occurs at a positive deflection angle.

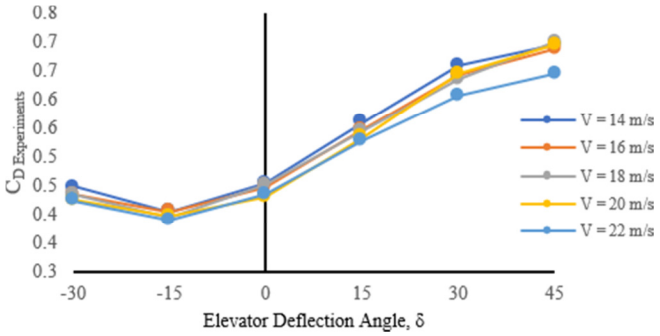

Fig. 15. Relationship of experimental C_D drag coefficient and change in elevator deflection angle δ at angle of attack α = -5° for each level of flow velocity change.

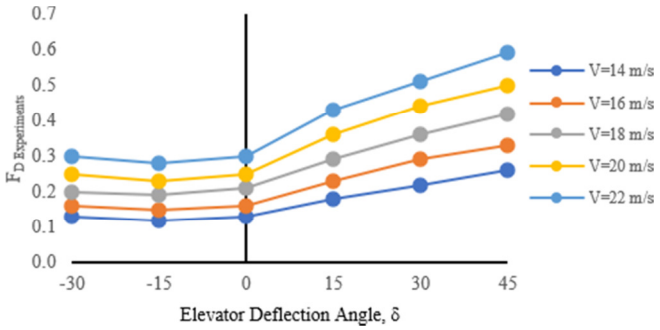

Fig. 16. Relationship of experimental drag force F_D and change in elevator deflection angle δ at an angle of attack α = -15° for each level of change in flow velocity.

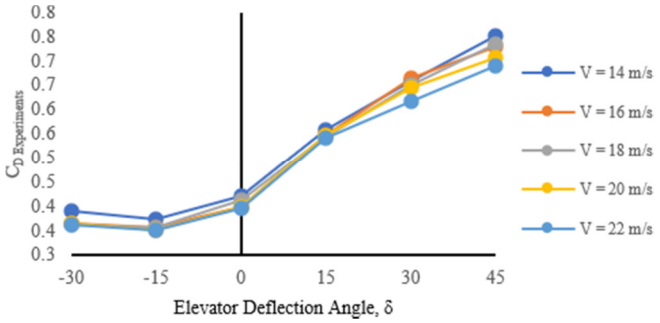

Fig. 17. Relationship between the experimental C_D drag coefficient and change in elevator deflection angle δ at angle of attack α = -1° for each level of flow velocity change.

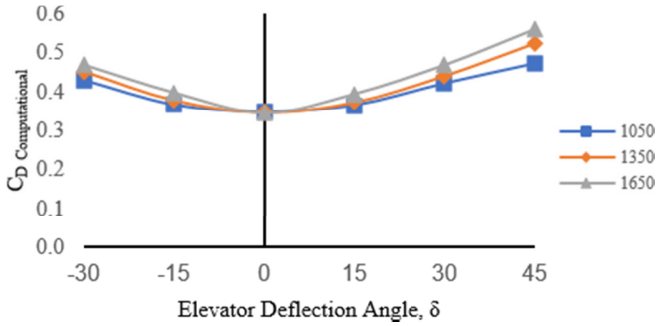

Fig. 18. Relationship between computed C_D drag coefficient and change in elevator deflection angle δ at angle of attack α = 0° and V = 22 m/s for each elevator width level.

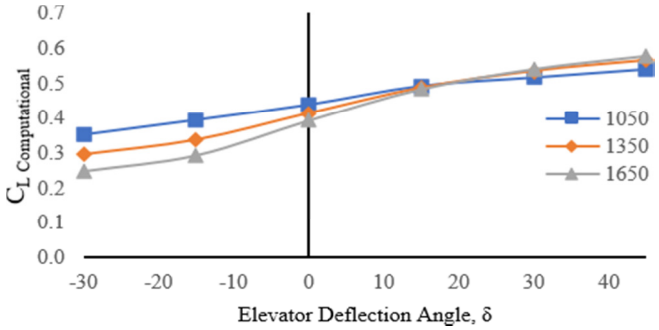

Fig. 19. Relationship between computed drag coefficient C_L and change in elevator deflection angle δ at angle of attack α = 0° and V = 22 m/s for each elevator width level.

Figures 18, 19, and 20 present the results of the numerical or computational simulations of the relationship between C_D, C_L, and $C_L/C_{D,}$ with elevator deflection angle δ for each level of elevator width (W) at an angle of attack α = 0° and airflow velocity V = 22 m/s. The characteristic pattern exhibited is the same for each level of elevator width, and obtains the largest C_D value of 0.561 N at δ = 45° and elevator width W = 1650 mm, the largest C_L value of 0.577 at δ = 45° and elevator width W = 1650 mm, and the C_L/C_D value = 1.352 at δ = 15° at elevator width W = 1050 mm. These computational results show a lower C_D value than the experimental value of $C_{D,Experiment}$ = 0.681. The exciting aspect of these computational results is that the largest C_L/C_D value is not obtained at δ = 45° and elevator width W = 1650 mm, indicating that neither the elevator width nor the deflection angle must be large.

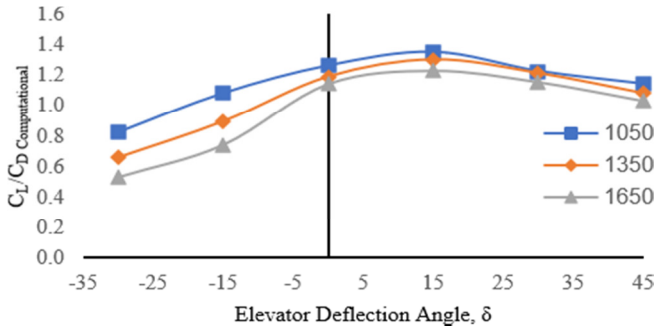

Fig. 20. Relationship between lift coefficient and computational drag coefficient C_L/C_D versus change in elevator deflection angle δ at angle of attack α = 0° and V = 22 m/s for each elevator width level.

Figure 21 depicts the relationship between the numerical, computational, and experimentally simulated C_D with elevator deflection angle δ for elevator width W = 1350 mm at angle of attack α = 0° and airflow velocity V = 22 m/s. The smallest C_D value for the experiment is 0.485, whereas the computational value is 0.522 at the same elevator angle, δ = 45°. The characteristic pattern demonstrated is similar, and the largest C_D value is obtained for the experiment of 0.645 N and computation of 0.522 at the same elevator angle δ = 45°. The smallest C_D value for the experiment is 0.485, while the computational value is 0.450 at the same elevator angle δ = -30°. The pressure coefficient of the PPH-Unhas aircraft model is presented in Figures 22–26. The treatments were given at elevator deflection angles δ = -30°, -15°, 0°, 15°, and 30°, with angle of attack α = 0°, airflow velocity V = 22 m/s, and elevator width W = 1350 mm. The obtained C_P values indicate the position of the flow separation on the horizontal stabilizer, elevator, and aircraft wing.

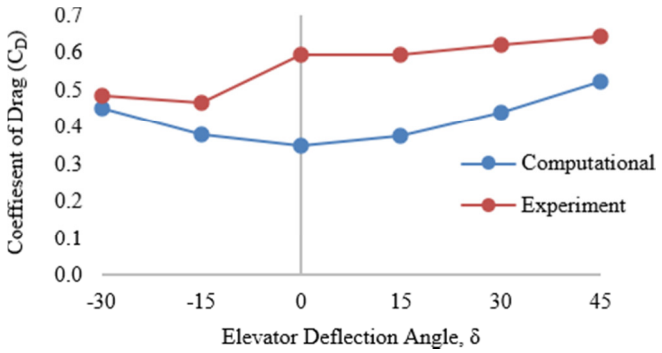

Fig. 21. Relationship between the computational and experimental C_D drag coefficients and change in elevator deflection angle δ at angle of attack α = 0° and V = 22 m/s for elevator width W = 1350 mm.

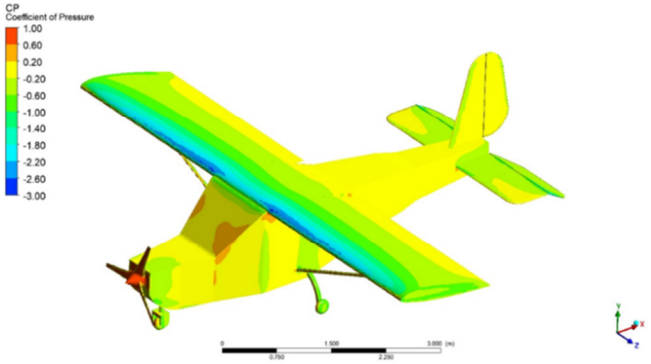

Fig. 22. The pressure coefficient (C_P) contour at the elevator deflection angle δ = -30° with angle of attack α = 0° and V = 22 m/s for an elevator width W = 1350 mm.

The pressure coefficient contour shows positive values on the horizontal stabilizer and elevator at the elevator deflection angles of 15° and 30°, which proves the occurrence of downward pressure on the tail of the aircraft so that the muzzle of the aircraft is lifted because, at the same time, the pressure coefficient on the upper surface of the wing is negative.

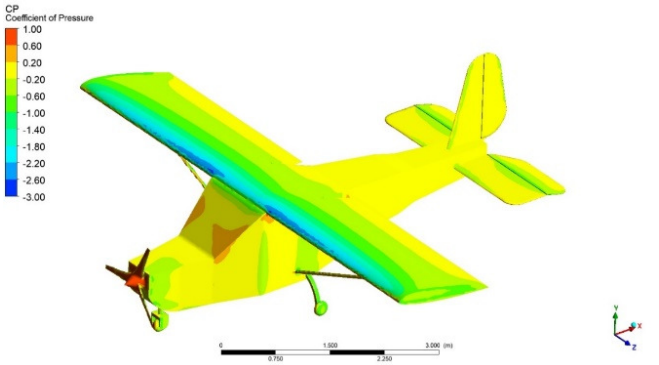

Fig. 23. The pressure coefficient (C_P) contour at the elevator deflection angle δ = -15° with angle of attack α = 0° and V = 22 m/s for an elevator width W = 1350 mm.

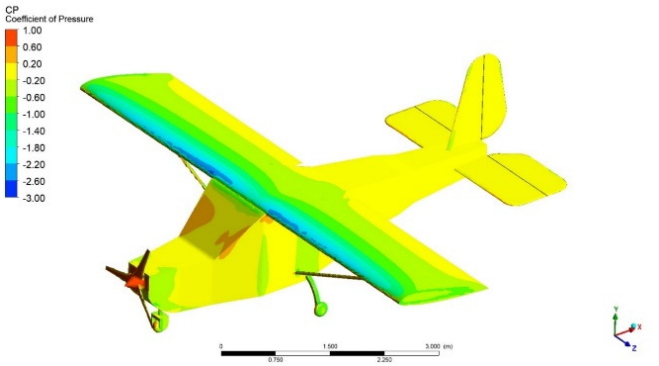

Fig. 24. The pressure coefficient (C_P) contour at the elevator deflection angle δ = 0° with angle of attack α = 0° and V = 22 m/s for an elevator width W = 1350 mm.

The pressure coefficient contour shows positive values on the horizontal stabilizer and elevator at the elevator deflection angles of 15° and 30°, which proves the occurrence of downward pressure on the tail of the aircraft so that the muzzle of the aircraft is lifted because, at the same time, the pressure coefficient on the upper surface of the wing is negative.

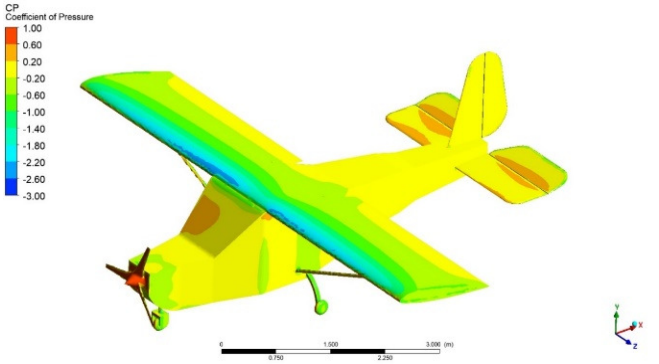

Fig. 25. The pressure coefficient (C_P) contour at the elevator deflection angle δ = 15° with angle of attack α = 0° and V = 22 m/s for an elevator width W = 1350 mm.

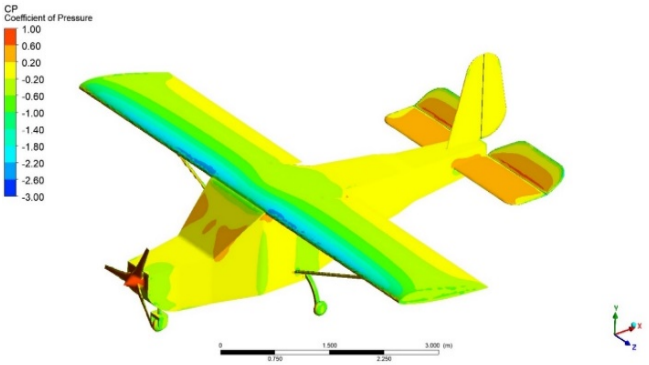

Fig. 26. The pressure coefficient (C_P) contour at the elevator deflection angle $\delta = 30°$ with angle of attack $\alpha = 0°$ and $V = 22$ m/s for an elevator width $W = 1350$ mm.

IV. CONCLUSIONS

This study presents an experimental and numerical simulation investigation into the drag force characteristics, drag coefficient, and lift coefficient resulting from the interaction of fluid flow with the horizontal stabilizer and elevator of the PPH-Unhas microlight aircraft. The experiments were conducted in a wind tunnel with variations in the free-stream velocity at five levels (14–22 m/s), elevator deflection angles at six levels (-30° to 45°), and angles of attack at seven levels (-15° to 25°). Meanwhile, numerical simulations were performed for three different elevator widths (1050, 1350, and 1650 mm), with a fixed angle of attack at $\alpha = 0°$ and an airflow velocity of $V = 22$ m/s.

The experimental results indicate that increasing the elevator deflection angle (δ) contributes to an increase in the drag force (F_D) and drag coefficient (C_D), as observed under conditions of $V = 22$ m/s and $\alpha = 0°$, where C_D increased from 0.593 ($\delta = 0°$) to 0.645 ($\delta = 45°$). A similar trend was observed in the numerical simulation results, where the C_D increased from 0.324 ($\delta = 0°$) to 0.560 ($\delta = 45°$). Furthermore, an increase in the deflection angle also affected the lift coefficient (C_L), which increased from 0.439 ($\delta = 0°$) to 0.577 ($\delta = 45°$). The C_L/C_D ratio reached its maximum value at $\delta = 15°$, indicating that this was the optimal angle for aerodynamic efficiency.

Compared with the experimental results, the numerical simulations exhibited a similar characteristic trend, with differences within an acceptable range. The highest C_D value recorded in the experiments was 0.645, whereas the computational value was 0.522 at $\delta = 45°$. The lowest C_D value in the experiments was 0.485, whereas the numerical value was 0.450 at $\delta = -30°$. The pressure distribution analysis based on the pressure coefficient (C_P) contours from the computational results revealed flow separation patterns that affected the aircraft's longitudinal stability. The dominance of positive pressure on the horizontal stabilizer and elevator at deflection angles of 15° and 30°, respectively, confirmed the presence of a downward force on the aircraft tail, causing the nose to rise.

The primary contribution of this study is the investigation of the effects of elevator deflection and size on the aerodynamic characteristics of a microlight aircraft, an aspect that has not been extensively explored in previous studies. In addition to providing an experimental validation of the numerical simulation results, this study introduces an analysis of elevator width variations on aerodynamic performance, which can serve as a reference for designing and optimizing longitudinal control systems in light aircraft. Consequently, this study offers new insights into microlight aircraft development and serves as a valuable reference for future studies on light aircraft aerodynamics.

ACKNOWLEDGMENT

The authors would like to express their gratitude to the Directorate of Research, Technology, and Community Service of the Ministry of Education, Culture, Research and Technology, and the Institute for Research and Community Service (LP2M) of Hasanuddin University, which financed the research through Regular Fundamental Research (PFR) with master contract number 050/ES/PG.02.00.PL/2024 and derivative contract number 02035/UN4.22.2/PT.01.03/2024, and to the manager of the Fluid Mechanics Laboratory of the Department of Mechanical Engineering, Faculty of Engineering, Hasanuddin University, who allowed and facilitated the implementation of this research.

REFERENCES

[1] A. Pelletier and T. J. Mueller, "Low Reynolds Number Aerodynamics of Low-Aspect-Ratio, Thin/Flat/Cambered-Plate Wings," *Journal of Aircraft*, vol. 37, no. 5, pp. 825–832, Sep. 2000, https://doi.org/10.2514/2.2676.

[2] N. Salam, R. Tarakka, Jalaluddin, D. Iriansyah, and M. Ihsan, "The Effects of Flap Angles on the Aerodynamic Performances of a Homebuilt Aircraft Wing Model," *International Journal of Mechanical Engineering and Robotics Research*, vol. 11, no. 12, pp. 908–914, 2022, https://doi.org/10.18178/ijmerr.11.12.908-914.

[3] R. Sepe, R. Citarella, A. De Luca, and E. Armentani, "Numerical and Experimental Investigation on the Structural Behaviour of a Horizontal Stabilizer under Critical Aerodynamic Loading Conditions," *Advances in Materials Science and Engineering*, vol. 2017, no. 1, 2017, Art. no. 1092701, https://doi.org/10.1155/2017/1092701.

[4] G. Nugroho, H. Sasongko, M. Adenan, Sarwono, and H. Mirmanto, "A CFD analysis of NACA 0015 airfoil as a horizontal stabilizer with gap length variations," *Journal of Energy, Mechanical, Material, and Manufacturing Engineering*, vol. 7, no. 2, pp. 75–82, 2022, https://doi.org/10.22219/jemmme.v7i2.26425.

[5] S. Ravikanth et al., "A Effect of Elevator Deflection on Lift Coefficient Increment," *International Journal of Modern Engineering Research*, vol. 5, no. 6, pp. 09–25, 2015.

[6] S. Mageshwaran, T. Banu, B. Manoharan, and M. Jeganathan, "Aerodynamic Analysis of Seamless Horizontal Stabilizer," *International Journal of Advanced Research in Engineering and Technology*, vol. 10, no. 6, pp. 561–572, Dec. 2019.

[7] A. K. Singh and R. Dahiya, "Dynamic Modeling and Control of Aircraft Surfaces Using Hybrid Intelligent Controllers," *IOSR Journal of Electrical and Electronics Engineering*, vol. 12, no. 6, pp. 21–40, 2018.

[8] O. M. Al-Habahbeh, M. Abu-Elola, L. Rousan, and M. A. Al-Khawaldeh, "Boosting Aircraft Efficiency by Reversing the Load on the Horizontal Stabilizer," *International Journal of Recent Technology and Engineering*, vol. 8, no. 3, pp. 112–119, Sep. 2019, https://doi.org/10.35940/ijrte.C3901.098319.

[9] R. Bardera, Á. A. Rodríguez-Sevillano, and E. Barroso, "Numerical and Experimental Study of Aerodynamic Performances of a Morphing Micro Air Vehicle," *Applied Mechanics*, vol. 2, no. 3, pp. 442–459, Sep. 2021, https://doi.org/10.3390/applmech2030025.

[10] J. Wang, X. Zhang, J. Lu, and Z. Tang, "Numerical Simulation and Experimental Study on the Aerodynamics of Propulsive Wing for a Novel Electric Vertical Take-Off and Landing Aircraft," *Aerospace*, vol. 11, no. 6, Jun. 2024, Art. no. 431, https://doi.org/10.3390/aerospace11060431.

[11] O. Al-Shamma, "An Instructive Algorithm for Aircraft Elevator Sizing to Be Used in Preliminary Aircraft Design Software," *Journal of Applied Engineering Science*, vol. 15, no. 4, pp. 489–494, Oct. 2017, https://doi.org/10.5937/jaes15-14829.

[12] S. Nithya and S. Kanimozhi, "Aerodynamic analysis of seamless horizontal stabilizer," *IOP Conference Series: Materials Science and Engineering*, vol. 197, no. 1, May 2017, Art. no. 012083, https://doi.org/10.1088/1757-899X/197/1/012083.

[13] H. Arrosida and M. E. Echsony, "Aircraft Pitch Control Design using Observer-State Feedback Control," *Kinetik*, vol. 2, no. 4, pp. 263–272, Sep. 2017, https://doi.org/10.22219/kinetik.v2i4.267.

[14] A. Dziubiński, P. Jaśkowski, and T. Seredyn, "CFD Analysis of Agricultural Aircraft Aerodynamic Characteristics," *Transactions of the Institute of Aviation*, vol. 245, no. 4, pp. 321–337, Dec. 2016, https://doi.org/10.5604/05096669.1229486.

[15] M. S. Genç, G. Özkan, H. H. Açikel, M. S. Kiriş, and R. Yildiz, "Effect of tip vortices on flow over NACA4412 aerofoil with different aspect ratios," *EPJ Web of Conferences*, vol. 114, 2016, Art. no. 02027, https://doi.org/10.1051/epjconf/201611402027.

[16] M. B. S. Pratama, E. Sulaeman, K. G. Walesasi, and A. Legowo, "Elevator Tab Model and Aerodynamic Hinge Moment Variation Effect on Flutter Analysis of a Small Commuter Aircraft," *CFD Letters*, vol. 14, no. 1, pp. 20–37, Jan. 2022, https://doi.org/10.37934/cfdl.14.1.2037.

[17] M. B. Zuhair, "Balancing an aircraft with symmetrically deflected split elevator and rudder during short landing run," *Aviation*, vol. 23, no. 1, pp. 23–30, May 2019, https://doi.org/10.3846/aviation.2019.10301.

[18] G. K. Ananda and M. S. Selig, "Stall/Post-Stall Modeling of the Longitudinal Characteristics of a General Aviation Aircraft," in *AIAA Atmospheric Flight Mechanics Conference*, Washington, D.C., USA, Jun. 2016, https://doi.org/10.2514/6.2016-3541.

[19] A. Srivastava, "Determination of Aerodynamic Forces and Control Requirement during Ground Effect," *International Journal of Aviation, Aeronautics, and Aerospace*, vol. 6, no. 4, Jan. 2019, Art. no. 15, https://doi.org/10.15394/ijaaa.2019.1413.

[20] J. D. Anderson Jr, *Aircraft Performance and Design*. McGraw-Hill Edition, 2010.

[21] Yunus A. Cengel and John M. Cimbala, *Fluid Mechanics Fundamental and Application*, Fourth Edition. McGraw-Hill Education, 2018.